ORIGINAL ARTICLE

Clinical Physiology and
Functional Imaging

Software development to optimize the minimal detectable difference in human airway images captured using optical coherence tomography

Carli M. Peters[1] | Robert C. Peters[1] | Anthony D. Lee[2] | Pierre Lane[2] | Stephen Lam[2] | Don D. Sin[3] | Donald C. McKenzie[1] | A. William Sheel[1]

[1]School of Kinesiology, Faculty of Education, University of British Columbia, Vancouver, Canada

[2]Department of Integrative Oncology, BC Cancer Research Institute, Vancouver, British Columbia, Canada

[3]Department of Medicine (Respirology), Centre for Heart Lung Innovation, St. Paul's Hospital, University of British Columbia, Vancouver, British Columbia, Canada

Correspondence
Carli Peters, School of Kinesiology, Faculty of Education, University of British Columbia, 2553 Wesbrook Mall, Vancouver, BC V6T 1Z3, Canada.
Email: carli.peters@alumni.ubc.ca

Abstract

Optical coherence tomography (OCT) is an imaging methodology that can be used to assess human airways. OCT avoids the harmful effects of ionizing radiation and has a high spatial resolution making it well suited for imaging the structure of small airways. Analysis of OCT airway images has typically been performed manually by tracing the airway with a relatively high coefficient of variation. The purpose of this study was to develop an analysis tool to reduce the inter- and intra-observer reproducibility of OCT and improve the ability to detect differences in airways. OCT images from healthy, young human volunteers were used to develop and test the OCT software. Measurement software was developed to allow the conversion of the original image into a grayscale image and was followed by an enhancement operation to brighten the image, and contour measurement. A total of 140 OCT images, 70 small (<2 mm) and 70 medium (2–4 mm) sized airways were analyzed. The inter- and intraobserver reproducibility of airway measurements ranged for strong to very strong in the small-sized airways. For medium-sized airways the reproducibility was considered moderate. Bland-Altman bias was low between observers and observations for all measures. The minimal detectable differences in the airway measurements with our semi-automated software were lower relative to manual tracing in medium-sized airways. Our software improves the ability to perform quantitative OCT analysis and may help to quantify the extent of airway remodelling in respiratory disease or elite athletes in future studies.

KEYWORDS
airway area; airway lumen; bronchi; lung, wall area percentage, wall thickness

1 | INTRODUCTION

The term airway remodelling describes structural changes in the airway wall caused by repeated injury and repair cycles. Remodelling is characterized by changes in tissue, cellular, and molecular composition of airway smooth muscle, extracellular matrix, epithelium, and vasculature (Hirota & Martin, 2013). Two types of airway remodelling, physiological and pathological, can be distinguished. Physiological airway remodelling describes structural changes that occur during normal lung development and lead to a normal airway

wall or transient injuries/inflammation that resolve and return to normal airway structure. Pathological airway remodelling results from disturbed lung development or as a response to chronic injury/ inflammation that lead to lasting alterations in airway wall structure (Fehrenbach et al., 2017). Pathological airway remodelling is a common feature of asthma and chronic obstructive pulmonary disease (COPD) (Jeffery, 2001). While not as well characterized as in chronic inflammatory diseases, remodelling also seems to occur in some elite athletes (Kippelen, et al., 2012).

Elite athletes sustaining high ventilations during exercise in unfavourable environmental conditions, such as cold dry air, polluted air, or chlorinated indoor pools, are prone to repeated airway epithelium injury (Bougault & Boulet, 2013; Rundell & Sue-Chu, 2013; Sue-Chu, 2012). Early work demonstrated that asthma and asthma-like symptoms are more common in competitive cross-country skiers than in nonskiers (Larsson et al., 1993). Biopsy specimens from the proximal airways in elite skiers without a diagnosis of asthma, subjects with mild asthma, and healthy controls demonstrated that skiers and asthmatics had an increased deposition of the extracellular matrix glycoprotein tenascin in the basement membrane (Karjalainen et al., 2000). Similarly, biopsy data from the segmental, subsegmental, and lobar airways have shown increased tenascin deposition and submucosal type I and type III collagen expression in elite swimmers compared to controls (Bougault et al., 2012). Whether or not the remodelling of airways in athletes is reversible upon cessation of competitive training is unclear (Bougault et al., 2018; Vergès et al., 2004). Evidence of deviations from normal healthy structure cannot be provided with certainty without quantitative analysis of airway structural components (Fehrenbach et al., 2017).

Airway structure can be assessed in multiple ways including histological analysis of biopsy samples (Bougault et al., 2012; Karjalainen et al., 2000), computed tomography (Grenier et al., 2002), and optical coherence tomography (OCT) (Coxson et al., 2008). Using OCT, images of the airways with a resolution of approximately 15 μm can be captured (Hanna et al., 2005; Huang et al., 1991) and unlike other in vivo techniques (e.g. CT and airway biopsies), OCT can evaluate medium to small-sized airways (i.e. airways less than 5 mm in diameter), which are the active sites of disease in airway conditions such as chronic obstructive pulmonary disease (COPD) and bronchiolitis (Coxson et al., 2008). Several anatomic airway measures, including luminal area (Ai), luminal diameter, the airway wall area percentage (WA%), and wall thickness (WT), can then be obtained from the OCT images (Ding et al., 2016; Kirby et al., 2015; Su et al., 2019). OCT measurements were originally validated in excised porcine airways matched to histological sections of the same specimen (Lee et al., 2014). More recently, human airway OCT-derived measures were validated by comparison with pathology up to the 9th generation bronchi (Chen et al., 2015). The work by Lee et al. (2014) and Chen et al. (2015) suggests OCT can provide an accurate measure of airway anatomy; however, the ability of OCT to be a helpful tool for measuring airway remodelling is dependent on the reproducibility of measurement techniques.

One method for analyzing OCT data involves manually tracing the inner and outer wall of consecutive OCT frames (Adams et al., 2019; Coxson et al., 2008; Kirby et al., 2015). The reproducibility of this technique and short-term insertion and reinsertion of OCT for evaluating the same airway has been evaluated, and a 12% coefficient of variation in insertion-reinsertion WT measures was found. A large portion of the variability was explained by the observer, as intra-observer coefficient of variation for repeated measures of the same airway was 9% (Kirby et al., 2015). The development of an analysis technique that improves the inter- and intraobserver reproducibility of OCT measures will allow airway remodelling studies in both patients and athletes to detect smaller differences in airway structure between control and experimental or treatment groups.

In this manuscript, we describe the development of software that can be utilized to semi-automate the process of measuring OCT-derived airway measures. Second, we demonstrate the intra- and interobserver reproducibility of this software using in-vivo images of small (<2 mm in diameter) and medium-sized (2–4 mm in diameter) airways acquired in healthy, nonsmoking adults. We also compare the intra-observer reproducibility using our software to the reproducibility of a manual tracing technique. Enhanced software and improved reproducibility will expand the ability to discern minimal detectable differences in OCT-derived airway measures. Our findings can be used to inform future studies investigating airway remodelling using OCT and to better understand clinically-relevant changes to human airways.

2 | METHODS

2.1 | Participants

The OCT images used to develop and test the reproducibility of the OCT software were obtained in healthy, young human volunteers. The subject characteristics and resting pulmonary function have been reported elsewhere (Peters et al., 2021). In brief, healthy females (n = 3) and males (n = 2) between the ages of 23–45 years with normal pulmonary function based on predicted values were included. In vivo imaging was approved by the Clinical Research Ethics Board of the University of British Columbia (approval number: H14-00724). All subjects were informed about the experimental procedures as well as the potential risks involved and provided written informed consent.

2.2 | Software overview

Software was developed using Visual Studio 2015, C# and OpenCV libraries to detect the luminal wall and airway wall (Figure 1). The workflow of the software is shown in Figure 2. Original images for a given pullback (see: *OCT image acquisition*), exported from MatLab with a fixed conversion factor of 0.0049761 mm/pixel, were opened in the software. Each image of the pullback was analyzed

independently with the following steps. The original image (Figure 2a) was converted to a grayscale image. This step simplified image processing with very little loss of information. The original image had three values for each pi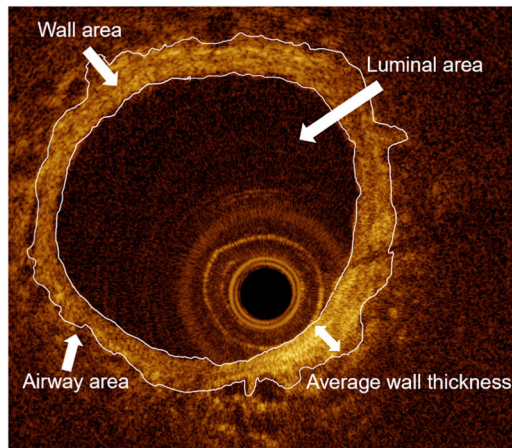xel; one each for the blue, green and red values used to create the image. A grayscale image has only one value for each pixel, so a formula has been developed to combine the three levels into one. The following standard conversion formula was used to convert the original image into a grayscale image:

$$\text{BGR to Gray} \leftarrow 0.114 \cdot B + 0.587 \cdot G + 0.299 \cdot R,$$

where B represents the blue value, G represents the green value, and R represents the red value in the original image. Figure 2b illustrates the results of the BGR to grayscale conversion. For clarity, the remainder of the software description will describe the steps used to detect the lumen only. The same remaining steps are used to detect the outer airway.

A low pass filter was then used to reduce the noise within the image using a blur operation. A median blur filter replaced each pixel in the grayscale image with the median value of the neighbouring pixels. A block size was used to determine how big the neighbourhood was. The block size was always a positive odd integer. For example, when a block size of 15 was used, the median value of all the pixels in a 15 × 15 pixel box and centred over the pixel of interest, was used to calculate the new pixel value in the blurred image. The median blur is performed on each pixel of the grayscale image. Figure 2c shows the result of applying a blur with a block size of 15 to Figure 2b.

An enhancement operation was sometimes performed to brighten the pixels as a function of the distance the pixel is from
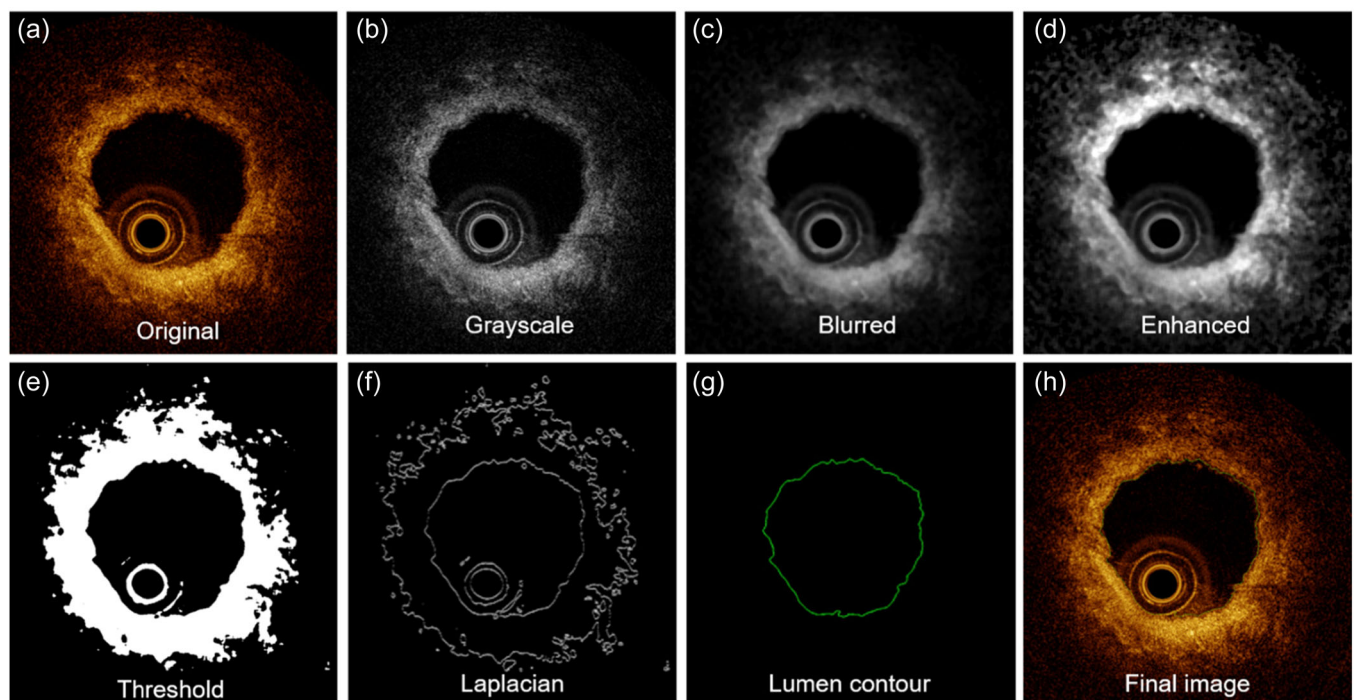

FIGURE 1 Optical coherence tomography (OCT) image highlighting the luminal wall and airway wall detected by the software. OCT-derived airway measures including airway luminal area, airway area, wall area, wall area percent, and wall thickness can be calculated after detecting the airway lumen and airway wall contours.

FIGURE 2 Steps used by imaging software to detect the airway lumen. (a) Shows the original optical coherence tomography (OCT) image. (b) Shows conversion of the original image to grayscale. (c) Shows the result of applying a 15 × 15 pixel median blur filter to the grayscale image. (d) Shows the result of enhancing the blurred image by a factor of 0.0001 to brighten the pixels further from the probe. (e) Shows the result of applying a threshold of 75 to the enhanced image. Any pixels ≥ the threshold were set to 255 (white) and any pixel values < the threshold were set to 0 (black). (f) Shows the result of performing a Laplacian operation to the threshold image to find contours. (g) Shows the lumen contour selected by the software. (h) Shows the original image with the lumen contour overlaid.

the centre of the image (location of the probe). A custom function was created to build an enhancement matrix for each pixel location in the image. The distance that each pixel is from the centre of the image is calculated by the formula:

$$Distance = \sqrt{(y - center\ y)^2 + (x - center\ x)^2}.$$

The enhancement value for each pixel is calculated by multiplying the user entered scaling factor by the square of the distance the pixel is from the centre of the image.

$$Enhancement\ matrix\ [y, x] = scaling\ factor \times distance \times distance.$$

When an enhancement was utilized, each pixel was reevaluated with the following function:

$$Pixel\ value = original\ value + (original\ value \times enhancement).$$

If the resulting value was greater than 255, the value is set to 255, the maximum value for an eight-bit pixel. Figure 2d shows the result of enhancing the blurred image in Figure 2c. In Figure 3, the original image, which has been converted to a grayscale image and blurred, is shown in panel A. Note that the left side of the airway lumen closest to the probe is brighter than the right side of the airway lumen. Also note that there is bronchial secretion surrounding the probe that is creating noise within the lumen. When a lumen

threshold is set without enhancing the pixels within the image based on distance from the probe, the software detects the far wall and the edge of the bronchial secretion as the airway lumen surface (Figure 3b). However, when an enhancement of 0.00001 is added to the blurred image (Figure 3c) and the threshold value is increased, the software detects the lumen surface accurately (Figure 3d). Enhancements were performed separately for lumen detection and airway detection. If enhancement of images was unnecessary, this step was not required.

A binary thresholding tool was then applied to the blurred (or enhanced) image. The binary thresholding tool looked at each pixel and determined whether its value was greater than or equal to the threshold value. If it was greater than or equal to the threshold value, the pixel was set to 255 (white). If the value was less than the threshold value, the pixel was set to 0 (black). The result was a black and white image. Figure 2e illustrates the changes to Figure 2d when a threshold of 75 was applied for the lumen. Laplacian edge detection was then used to generate candidate contours for the lumen surface on the black and white image. The Laplacian operation calculates the second derivative associated with each pixel location. Figure 2f shows the image transformation when a Laplacian operation is applied. The FindContours function then extracted contours within the Laplacian image. To find the luminal surface, the area of each contour was calculated to find the smallest closed contour that encloses an area greater than 15 000 square pixels. The minimum helps to remove small contours seen in Figure 2f from consideration. Figure 2e shows the luminal wall contour in green on a blank image.
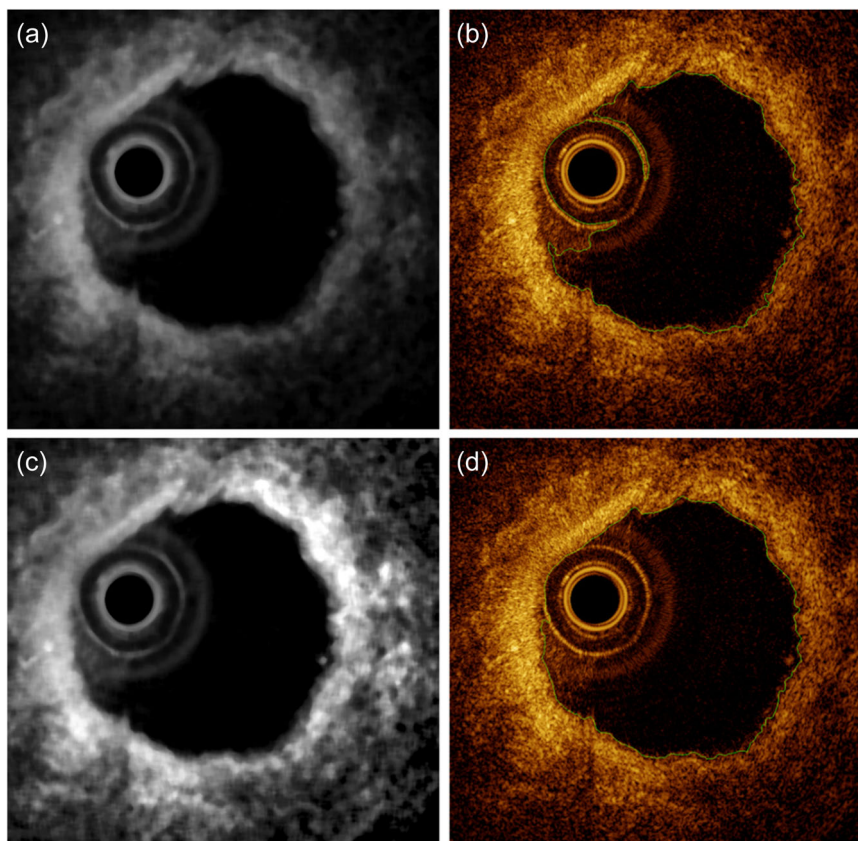

FIGURE 3 An example optical coherence tomography (OCT) image requires the use of a software enhancement tool. (a) Shows a grayscale and blurred image. When a threshold is applied to this image, the far luminal wall is detected accurately but the software incorrectly detects the edge of the probe and saliva as the luminal surface on the left-hand side of the airway in (b). (c) Shows the grayscale and blurred image with an enhancement applied. Enhancing the image and increasing the threshold allows both the far side of the luminal surface and the side closest to the probe to be detected accurately.
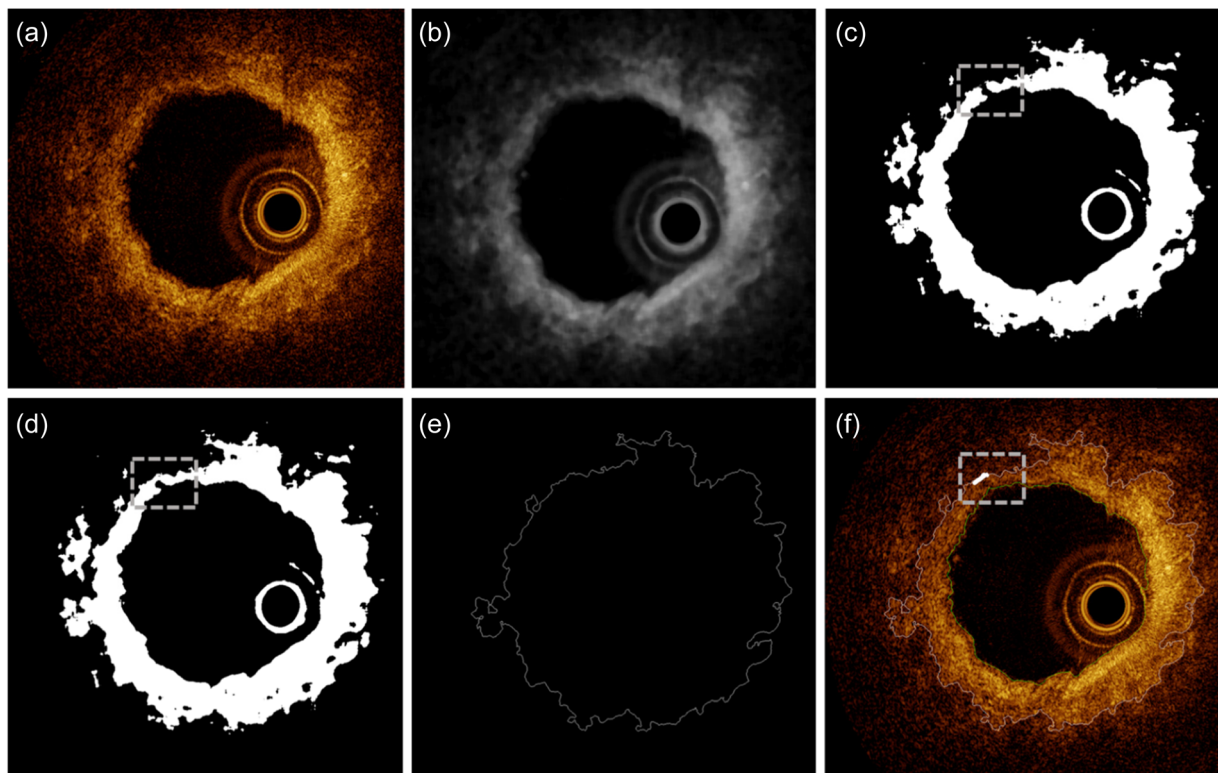
FIGURE 4 Demonstration of how the software's draw tool can be used to close a gap in the airway contour. (a) Shows the original optical coherence tomography image and (b) shows the image after it is converted to grayscale and filtered with a median blur. (c) Shows the result of applying a threshold to the image. Note the break in the airway wall within the grey box. (d) Shows the result of using the draw tool to close the break in the airway wall within the grey box. (e) Shows the outer airway the software has found after using a Laplacian operation. (f) Shows the original image with the luminal contour in green and the airway wall in white. The drawing to close the outer airway is shown in white within the grey box.

The results of the software operations are drawn onto the source image and displayed in Figure 2h. The block size used by the median blur filter, the enhancement value, and the threshold value were altered to adjust the final contour display until the observer thought the detected luminal contour lined up with the luminal surface.

The outer airway contour was detected simultaneously using the same operations described above. The blur, enhancement, and threshold values were set independently for detecting the outer airway contour, as sometimes different settings were required than for the luminal contour. When the FindContours function was used to extract contours from the Laplacian image, the largest closed contour surrounding the probe was picked as the outer airway contour.

When small breaks were present in the luminal surface or airway wall, as shown in Figure 4, a draw function was used on the source image to fix the break. The break in the airway wall in Figure 4a becomes clearer when the image is converted to grayscale and blurred in Figure 4b. Once a threshold is applied, as seen in Figure 4c, the break in the wall is very clear within the grey box. When the draw tool was used to fix the break, the drawing appeared as a white line on the image (Figure 4d). The drawing was kept as a separate image named the overlay image. This allowed the overlay to be cleared if the observer made a mistake with the drawing tool. Once the break was closed, the overlay image was combined with the original image, and the combined image was then processed with the remaining software steps. Figure 4e shows the outer airway contour that was detected after the break in the outer airway was closed using the draw tool. Figure 4f shows the contour image combined with the original image in Figure 4a, with the drawing fixing the break shown within the grey box.

2.3 | Calculating airway measures of interest within the software

The area of the lumen (Ai) and airway (Aa) was calculated using the ContourArea function which returned the area of the luminal and outer airway contour in square pixels. This value was then multiplied by the square of the conversion factor of 0.0049761 mm/pixel. The area of the airway wall (WA) was calculated by subtracting Ai from Aa (WA = Aa − Ai). Wall area % was calculated with the following equation:

$$\text{Wall area \%} = \frac{WA}{Ai + WA} \times 100\%.$$

The diameter of the lumen and airway were calculated by assuming the luminal and outer airway contours are a circle. The following formulas were used for diameter calculations:

$$\text{Lumen diameter} = 2\sqrt{\frac{Ai}{\pi}}.$$

$$\text{Airway diameter} = 2\sqrt{\frac{Aa}{\pi}}.$$

Wall thickness (WT) was calculated by subtraction of lumen radius from airway radius.

2.4 | OCT image acquisition

In vivo imaging was obtained using a custom-built 0.9 mm diameter OCT rotary-pullback catheter. The catheter was inserted through the biopsy channel of a bronchoscope into segmental airways in the upper and lower lobes of the right lung. After advancing the catheter into the airway until the internal diameter of the airway was the same as the catheter, 7 cm pullbacks were performed. An OCT system that employed a 50 kHz swept-source laser (SSOCT-1310, Axsun Technologies Inc.) was used for image acquisition. The pullback speed was set to 5 mm·s⁻¹ and the probe rotated at 49 Hz. To assess the intra-observer reproducibility of all OCT measures of interest using our software, a single observer measured a sample of 140 OCT images (70 with a luminal diameter <2 mm and 70 with a luminal diameter of 2–4 mm in diameter) on two occasions separated by 48 h. The same trained observer also measured the 140 OCT images on two occasions separated by 48 h using ImageJ (National Institutes of Health) to manually trace the inner and outer airway walls. To evaluate the interobserver reproducibility of our software, a second observer measured variables of interest in the same sample of OCT images.

2.5 | Statistics

Intra- and interobserver measurement reproducibility were determined using Pearson correlation coefficients and Bland-Altman analysis. For the observer that performed repeated measurements, the intraobserver measurement intraclass correlation coefficient (ICC) (SPSS Statistics 28) and coefficient of variation were also generated. Using the intra-observer ICC, the standard error of the measurement (SEM) for each airway variable was calculated using the following equation:

$$\text{SEM} = \text{SD}_{\text{Observation 1}} \times \sqrt{1 - \text{ICC}_{\text{Observation 1–Observation 2}}}.$$

The minimal detectable difference (MDD) for each airway variable was then calculated as:

$$\text{MDD} = 1.96 \times \sqrt{2} \times \text{SEM}.$$

A p value of <0.05 was considered statistically significant. Values are presented as means ± standard deviation.

3 | RESULTS

3.1 | Participants

The subjects in the present investigation completed a study that has been previously published (Peters et al., 2021) (Table S1). All subjects had a normal pulmonary function.

3.2 | Inter- and intraobserver reproducibility

A total of 140 OCT images, 70 small (<2 mm) and 70 medium (2–4 mm) sized airways, were analyzed. Table 1 shows interobserver measurement reproducibility of all OCT-derived airway measurements for small and medium-sized airways. The correlation coefficients for Ai were very strong for both small and medium-sized airways. For WA and WA% measures, the

TABLE 1 Interobserver measurement reproducibility of all OCT-derived airway measures using semi-automated software.

	Correlation		Bland–Altman	
	r	p	Bias	95% CI
<2 mm diameter				
Ai, mm²	0.997	<0.0001	0.0018 (0.0436)	−0.0836 to 0.0872
WA, mm²	0.961	<0.0001	0.0187 (0.1447)	−0.2649 to 0.3022
WA%, %	0.904	<0.0001	0.5384 (3.0484)	−5.4365 to 6.5133
WT, mm	0.916	<0.0001	0.0026 (0.0260)	−0.0482 to 0.0535
2–4 mm diameter				
Ai, mm²	0.999	<0.0001	0.0526 (0.1195)	−0.1816 to 0.2868
WA, mm²	0.768	<0.0001	−0.5087 (0.7400)	−1.9591 to 0.9417
WA%, %	0.766	<0.0001	−2.5623 (3.7700)	−9.9514 to 4.8269
WT, mm	0.360	0.0026	−0.0389 (0.0583)	−0.1531 to 0.0753

Abbreviations: Ai, luminal area; CI, confidence interval; OCT, optical coherence tomography; WA, wall area; WA%, wall area %; WT, wall thickness.
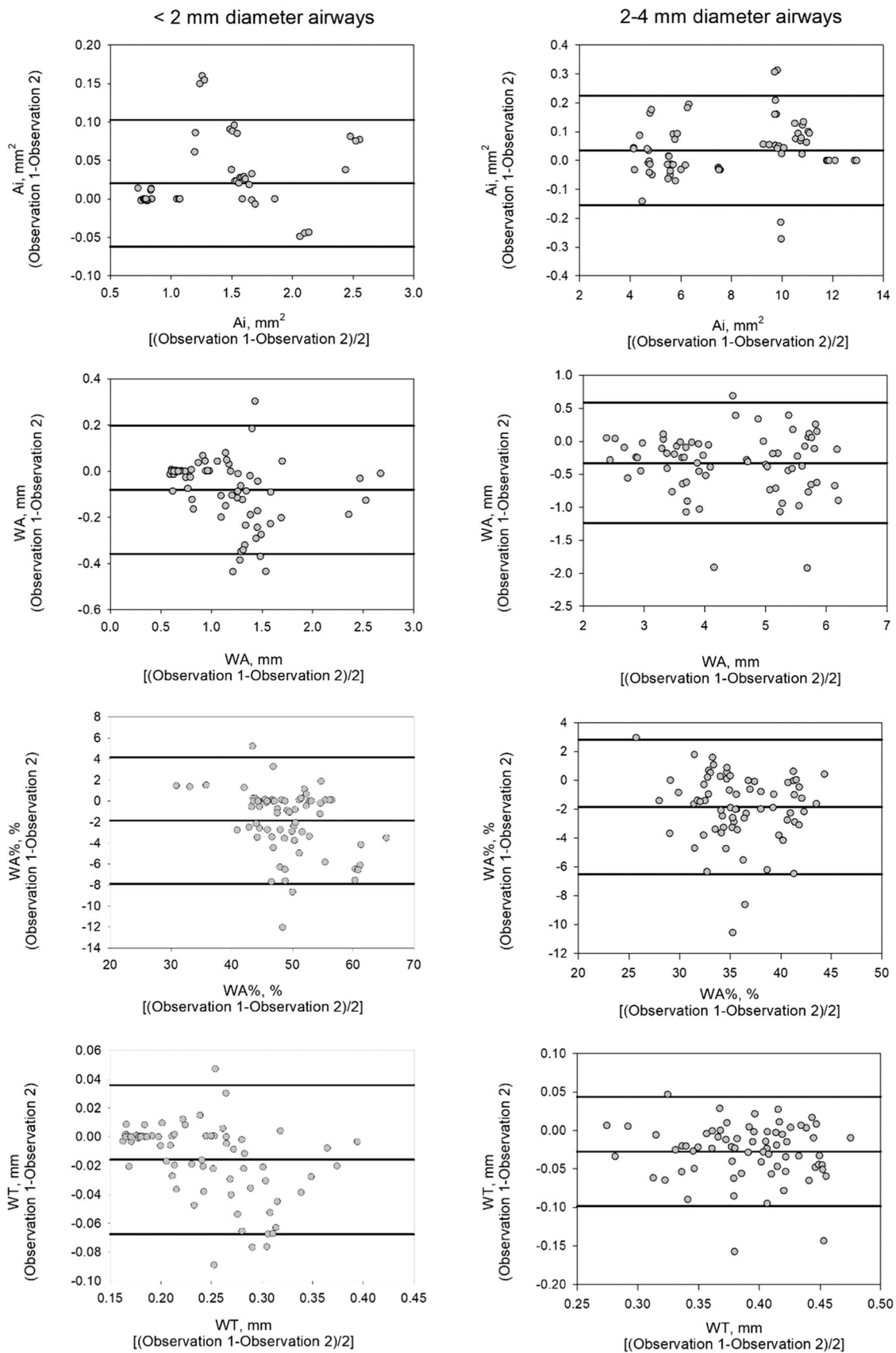
FIGURE 5 Intraobserver reproducibility of OCT-derived airway measures in small and medium-sized airways using semi-automated software. Ai, luminal area; OCT, optical coherence tomography; WA, wall area; WA%, wall area %; WT, wall thickness.

TABLE 2 Intraobserver measurement reproducibility of OCT-derived airway measures using semi-automated software.

	Correlation		Bland–Altman	
	r	p	Bias	95% CI
<2 mm diameter				
Ai, mm^2	0.997	<0.0001	0.0203 (0.042)	−0.0618 to 0.1025
WA, mm^2	0.959	<0.0001	−0.0804 (0.1414)	−0.3575 to 0.1966
WA%, %	0.897	<0.0001	−1.861 (3.076)	−7.8892 to 4.1671
WT, mm	0.918	<0.0001	−0.0158 (0.026)	−0.0674 to 0.0359
2-4 mm diameter				
Ai, mm^2	0.999	<0.0001	0.0354 (0.0966)	−0.1539 to 0.2247
WA, mm^2	0.915	<0.0001	−0.3287 (0.4657)	−1.2415 to 0.5841
WA%, %	0.841	<0.0001	−1.8541 (2.3793)	−6.5175 to 2.8093
WT, mm	0.729	<0.0001	−0.0274 (0.0362)	−0.0984 to 0.0436

Abbreviations: Ai, luminal area; CI, confidence interval; OCT, optical coherence tomography; WA, wall area; WA%, wall area %; WT, wall thickness.

correlation coefficients were very strong for small airways and moderate for medium-sized airways. In small airways, the correlation coefficient for WT was very strong, but for medium-sized airways the correlation coefficient was fair. Bland-Altman bias was low between observers for all measures (Figure 5). Table 2 shows intraobserver measurement reproducibility of all OCT-derived airway measurements for small and medium-sized airways using our measurement software. Correlation coefficients were very strong for Ai, WA, and WA% for small and medium-sized airways. For WT, correlation coefficients were very strong for small and moderate for medium-sized airways. Bland-Altman bias was low between observations for all measures (Figure 6).

3.3 | Small versus medium-sized airway reproducibility

Inter- and intra-reproducibility of OCT measures determined using Pearson's correlation coefficients were stronger in small compared to medium-sized airways in all measures except Ai (Tables 1 and 2). Coefficients of variation between observations were also larger for WA, WA%, and WT in medium-sized airways compared to small airways using software measurements or manual tracing. Measures of Ai had a larger coefficient of variation in small compared to medium-sized airways using both measurement techniques. When comparing measurement techniques in small airways, the coefficient of variation was larger for the manual tracing technique for Ai and WA% measures and smaller for WA and WT measures compared to measurement software. In the medium-sized airways, the coefficient of variation for all airway measures was larger when using the manual tracing technique compared to our software. The minimal detectable differences in the airway measurements are shown in Table 3.

4 | DISCUSSION

We have presented the development and reproducibility of software designed to make OCT-derived airway measures in humans. The major finding of this study is that compared with manually tracing the luminal surface and airway wall, the developed software has a smaller coefficient of variation in medium-sized airways and can therefore detect smaller differences in several OCT airway measures between groups of interest in future airway remodelling studies. The methodological advance described in this manuscript serves to enhance the capacity of those researchers interested in clinical and research applications of OCT.

A commonly used measurement technique for OCT airway images involves manually tracing the inner and outer airway wall using ImageJ software. Utilizing ImageJ, the coefficient of variation was 9% between repeated WT measures of the peripheral airways (airways with an Ai of ~1.8 mm^2) by the same trained observer in a group of current and former smokers (Kirby et al., 2015). In our study, the intraobserver coefficient of variation for WT measures of small airways (<2 mm in diameter with an average Ai of 1.2 mm^2) was 5.1% using the manual tracing technique and 5.4% using our software. Previous imaging work in heavy smokers at risk of or with COPD has shown that WT measures made in airways <2 mm were significantly greater in women compared to men and averaged 1.03 ± 0.13 mm and 0.93 ± 0.16 mm, respectively (Tam et al., 2016). The minimal detectable difference was slightly smaller for the manual tracing technique compared to our software (0.015 mm vs. 0.023 mm), but both techniques would be able to detect the small airway WT differences between women and men previously reported by Tam et al. (2016). The intraobserver coefficient of variation for WT measures of medium-sized airways (2–4 mm in diameter with an average Ai of 8.2 mm^2) was 10.8% using the manual tracing technique and 6% using our software (Table 3). A reduction in the coefficient of variation for WT measures in medium-sized airways
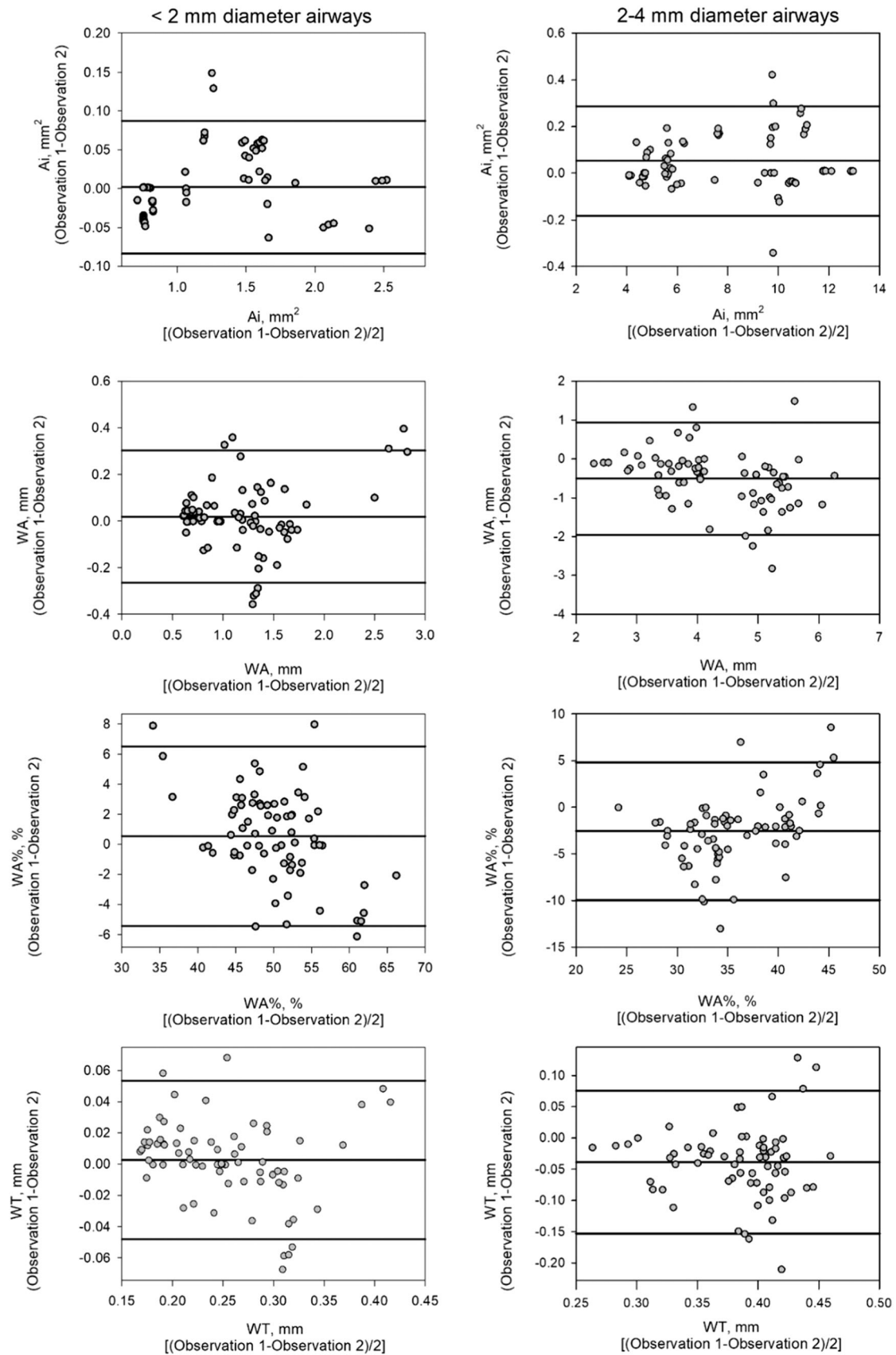
FIGURE 6 Interobserver reproducibility of OCT-derived airway measures in small and medium-sized airways using semi-automated software. Ai, luminal area; OCT, optical coherence tomography; WA, wall area; WA%, wall area %; WT, wall thickness.

TABLE 3 Minimal detectable differences in airway measurements between observations using semi-automated software and manual tracing techniques.

Technique	Intraobserver ICC	Coefficient of variation (%)	Standard error of the measurement	Minimal detectable difference
Software				
<2 mm diameter				
Ai	0.997	1.2	0.002 mm^2	0.006 mm^2
WA	0.956	5.9	0.030 mm^2	0.082 mm^2
WA%	0.884	3.4	1.048%	2.904%
WT	0.901	5.4	0.008 mm	0.023 mm
2–4 mm diameter				
Ai	0.999	0.7	0.003 mm^2	0.008 mm^2
WA	0.914	6.6	0.137 mm^2	0.379 mm^2
WA%	0.839	4.4	0.955%	2.646%
WT	0.727	6.0	0.019 mm	0.052 mm
Manual tracing				
<2 mm diameter				
Ai	0.998	1.8	0.002 mm^2	0.004 mm^2
WA	0.975	5.6	0.017 mm^2	0.048 mm^2
WA%	0.91	4.6	0.94%	2.606%
WT	0.938	5.1	0.005 mm	0.015 mm
2–4 mm diameter				
Ai	0.999	1.1	0.005 mm^2	0.013 mm^2
WA	0.758	10.5	0.422 mm^2	1.169 mm^2
WA%	0.664	6.8	2.403%	6.661%
WT	0.397	10.8	0.058 mm	0.161 mm

Abbreviations: Ai, luminal area; ICC, intraclass correlation coefficient; WA, wall area; WA%, wall area %; WT, wall thickness.

using our semi-automated software compared with manually tracing airways should allow the detection of smaller WT differences between groups of interest with fewer subjects required in future airway remodelling studies.

To date, airway remodelling assessed using OCT has largely focused on current and former smokers at risk or with COPD and asthmatics (Coxson et al., 2011). In 2015, OCT was used to compare Ai and WA measures in the seventh-ninth generation airways of never smokers, smokers without lung disease, and smokers with COPD (Chen et al., 2015). Differences in Ai and WA between never smokers and smokers without lung disease ranged from 1.23 to 1.76 mm^2 and $1.58–3.15 \text{ mm}^2$ in the seventh-ninth generations, respectively. More recently, OCT was used to measure Ai and WA of the third-ninth generation bronchi in patients with different stages of COPD, heavy smokers with a normal FEV_1, and healthy never smokers. The differences in Ai between healthy controls and heavy smokers with normal lung function was 2.1 mm^2 in the third-sixth airway generations and 1.5 mm^2 in the seventh-ninth airway generations. Values for WA differed by 2.25 mm^2 in the third-sixth

airway generations and 0.75 mm^2 in the seventh-ninth airway generations between healthy controls and heavy smokers with normal lung function (Ding et al., 2016). The MDD for Ai and WA measures (Table 3) using our software is such that it would be possible to detect differences in these measures between groups of the magnitude presented in the two studies mentioned above. While we are aware that chronic exercise training is a very different stimulus than smoking, airway remodelling has been demonstrated in athletes maintaining high levels of ventilation, particularly those that train and compete in cold or polluted air (Kippelen & Anderson, 2012).

Biopsy data in athletes suggests that airway remodelling occurs in highly trained cross-country skiers and swimmers. Increased tenascin expression in the subepithelial basement membrane in both cross-country skiers and swimmers and increased collagen I and III expression in swimmers' airways are similar to individuals with asthma (Bougault et al., 2012; Karjalainen et al., 2000). Whether this airway remodelling is physiological and transient in nature due to injuries/inflammation associated with elite sports training and

resolves after retirement from sport is unclear. In biopsies taken from six swimmers before and 2 years after retirement, collagen III expression was higher in retirement than during swim training and tenascin expression was unchanged after retirement. In the same study, lymphocytes and neutrophils were significantly reduced in all swimmers after retirement suggesting reversibility of bronchial inflammation that was present during a swim career (Bougault et al., 2018). The application of OCT imaging used in conjunction with our semi-automated software can be used to address whether airway remodelling in elite athletes is reversible. Unlike biopsies, OCT can provide high-resolution images of multiple airway generations in vivo during a single pullback without the need for tissue removal. This would allow for serial imaging of the same airways throughout an athletic career and into retirement. As evidence of airway remodelling in cross-country skiers and swimmers was previously found in biopsies taken from the larger/more proximal airways (lobar, segmental, and subsegmental airway generations) the reduced coefficient of variation of our software compared to manual tracing in medium-sized airways (Table 3) will aid in the detection of potentially small changes throughout an athletic career.

Building on the knowledge gained from biopsy data, OCT could offer further insight into airway remodelling in athletes. The ability of OCT to provide in vivo measures of airway walls across multiple generations without exposure to radiation makes it an appealing technique to study airway remodelling in both patient populations and healthy young athletes. The improved reproducibility of OCT measures made in medium-sized airways with the semi-automated software presented in this manuscript will hopefully enable the detection of, potentially subtle, airway changes due to remodelling in disease and sport.

ACKNOWLEDGMENTS

CONFLICTS OF INTEREST

The authors declare no conflicts of interest.

DATA AVAILABILITY STATEMENT

The data that support the findings of this study are available on request from the corresponding author. The data are not publicly available because of privacy and ethical restrictions.

REFERENCES

Adams, D.C., Miller, A.J., Applegate, M.B., Cho, J.L., Hamilos, D.L., Chee, A. et al. (2019) Quantitative assessment of airway remodelling and response to allergen in asthma. *Respirology*, 24, 1073–1080.

Bougault, V. & Boulet, L.P. (2013) Airways disorders and the swimming pool. *Immunology and Allergy Clinics of North America*, 33, 395–408.

Bougault, V., Loubaki, L., Joubert, P., Turmel, J., Couture, C., Laviolette, M. et al. (2012) Airway remodeling and inflammation in competitive swimmers training in indoor chlorinated swimming pools. *Journal of Allergy and Clinical Immunology*, 129, 351–358.

Bougault, V., Odashiro, P., Turmel, J., Orain, M., Laviolette, M., Joubert, P. et al. (2018) Changes in airway inflammation and remodelling in swimmers after quitting sport competition. *Clinical and Experimental Allergy*, 48, 1748–1751.

Chen, Y., Ding, M., Guan, W.J., Wang, W., Luo, W.Z., Zhong, C.H. et al. (2015) Validation of human small airway measurements using endobronchial optical coherence tomography. *Respiratory Medicine*, 109, 1446–1453.

Coxson, H.O., Eastwood, P.R., Williamson, J.P. & Sin, D.D. (2011) Phenotyping airway disease with optical coherence tomography. *Respirology*, 16, 34–43.

Coxson, H.O., Quiney, B., Sin, D.D., Xing, L., McWilliams, A.M., Mayo, J.R. et al. (2008) Airway wall thickness assessed using computed tomography and optical coherence tomography. *American Journal of Respiratory and Critical Care Medicine*, 177, 1201–1206.

Ding, M., Chen, Y., Guan, W.J., Zhong, C.H., Jiang, M., Luo, W.Z. et al. (2016) Measuring airway remodeling in patients with different COPD staging using endobronchial optical coherence tomography. *Chest*, 150, 1281–1290.

Fehrenbach, H., Wagner, C. & Wegmann, M. (2017) Airway remodeling in asthma: what really matters. *Cell and Tissue Research*, 367, 551–569.

Grenier, P.A., Beigelman-Aubry, C., Fétita, C., Prêteux, F., Brauner, M.W. & Lenoir, S. (2002) New frontiers in CT imaging of airway disease. *European Radiology*, 12, 1022–1044.

Hanna, N., Saltzman, D., Mukai, D., Chen, Z., Sasse, S., Milliken, J. et al. (2005) Two-dimensional and 3-dimensional optical coherence tomographic imaging of the airway, lung, and pleura. *Journal of Thoracic and Cardiovascular Surgery*, 129, 615–622.

Hirota, N. & Martin, J.G. (2013) Mechanisms of airway remodeling. *Chest*, 144, 1026–1032.

Huang, D., Swanson, E.A., Lin, C.P., Schuman, J.S., Stinson, W.G., Chang, W. et al. (1991) Optical coherence tomography. *Science*, 254, 1178–1181.

Jeffery, P.K. (2001) Remodeling in asthma and chronic obstructive lung disease. *American Journal of Respiratory and Critical Care Medicine*, 164, S28–38.

Karjalainen, E.M., Laitinen, A., Sue-Chu, M., Altraja, A., Bjermer, L. & Laitinen, L.A. (2000) Evidence of airway inflammation and remodeling in ski athletes with and without bronchial hyperresponsiveness to methacholine. *American Journal of Respiratory and Critical Care Medicine*, 161, 2086–2091.

Kippelen, P. & Anderson, S.D. (2012) Airway injury during high-level exercise. *British Journal of Sports Medicine*, 46, 385–390.

Kippelen, P., Fitch, K.D., Anderson, S.D., Bougault, V., Boulet, L.P., Rundell, K.W. et al. (2012) Respiratory health of elite athletes - preventing airway injury: a critical review. *British Journal of Sports Medicine*, 46, 471–476.

Kirby, M., Ohtani, K., Nickens, T., Lisbona, R.M., Lee, A.M., Shaipanich, T. et al. (2015) Reproducibility of optical coherence tomography airway imaging. *Biomedical Optics Express*, 6, 4365–4377.

Larsson, K., Ohlsén, P., Larsson, L., Malmberg, P., Rydström, P.O. & Ulriksen, H. (1993) High prevalence of asthma in cross country skiers. *BMJ*, 307, 1326–1329.

Lee, A.M., Kirby, M., Ohtani, K., Candido, T., Shalansky, R., MacAulay, C. et al. (2014) Validation of airway wall measurements by optical coherence tomography in porcine airways. *PLoS One*, 9, e100145.

Peters, C.M., Molgat-Seon, Y., Dominelli, P.B., Lee, A.M.D., Lane, P., Lam, S. et al. (2021) Fiber optic endoscopic optical coherence tomography (OCT) to assess human airways: the relationship between anatomy and physiological function during dynamic exercise. *Physiological Reports*, 9, e14657.

Rundell, K.W. & Sue-Chu, M. (2013) Air quality and exercise-induced bronchoconstriction in elite athletes. *Immunology and Allergy Clinics of North America*, 33, 409–421.

Su, Z.Q., Guan, W.J., Li, S.Y., Feng, J.X., Zhou, Z.Q., Chen, Y. et al. (2019) Evaluation of the normal airway morphology using optical coherence tomography. *Chest*, 156, 915–925.

Sue-Chu, M. (2012) Winter sports athletes: long-term effects of cold air exposure. *British Journal of Sports Medicine*, 46, 397–401.

Tam, A., Churg, A., Wright, J.L., Zhou, S., Kirby, M., Coxson, H.O. et al. (2016) Sex differences in airway remodeling in a mouse model of chronic obstructive pulmonary disease. *American Journal of Respiratory and Critical Care Medicine*, 193, 825–834.

Vergès, S., Flore, P., Blanchi, M.P. & Wuyam, B. (2004) A 10-year follow-up study of pulmonary function in symptomatic elite cross-country skiers: athletes and bronchial dysfunctions. *Scandinavian Journal of Medicine & Science in Sports*, 14, 381–387.

SUPPORTING INFORMATION

Additional supporting information can be found online in the Supporting Information section at the end of this article.